SAND2022-8070C

Metastability of Pulse Power Loads with Nonlinear Coupled Magnetics

Chaitanya S. Inamdar[1], Wayne W. Weaver[1], Rush D. Robinett III[1], David G. Wilson[2]
[1]Michigan Technological University, Houghton, MI 49931, USA,
[2]Sandia National Labs, Albuquerque, New Mexico 87123, USA
Email: csinamda@mtu.edu, wwweaver@mtu.edu, rdrobine@mtu.edu, dwilso@sandia.gov

***Abstract*—Pulse power loads are becoming increasingly more common in many applications primarily due to applications like radar, lasers and the technologies such as EMALS (Electro-Magnetic Aircraft Launch Systems) on next generation aircraft carriers. Pulse power loads are notorious for causing stability issues. Stability for pulse power loads can be defined to be *metastable*, where the system can be unstable for a portion of the pulse as long as the stability is re-established over the entire pulse. Dynamic characteristics for step changes in load can be improved with a modified boost converter topology in conjunction with bang-bang control. Improvement in the *metastability* margins will be presented through simulations with the application of the modified topology to pulse power loads.**

***Index Terms*—Coupled inductors, nonlinear inductor model, pulse load, constant power, stability.**

I. Introduction

Pulse power loads like radars and lasers are applied in a wide range of use cases. Niche applications like EMALS are also gaining traction. Pulse power loads cause a lot of stability issues in the systems they are deployed in [1], [2], [3]. Stability for pulsed power loads can be defined as metastable as bus voltage oscillations may grow during a period of instability but dampen during a period of stability and keep the voltage within bounds. According to the Hamiltonian Surface Shaping Power Flow Control (HSSPFC) method in [4], stability can be determined from the time derivative of the Hamiltonian. If the energy being generated and being dissipated are equal over a certain time period, a limit cycle is said to have occurred. The length of the limit cycle may not be the same as the switching period of the pulse power load. If the energy generated is more than the energy dissipated over the cycle period, the states will grow unbounded, and the system is unstable. Similarly, if the energy dissipated is greater than the energy generated, the state trajectories will decay, and the system is stable. Metastability margins can be mapped over a wide range of power levels and time periods with the maximum pulse duty cycle for which the system is stable marking the stability margin [5], [6]. In previous research, a linear inductor boost converter with constant duty cycle control is used to map the metastability margins [5]. This poses a question – Is an increase in metastability margins possible with a different control strategy and topology? This paper attempts to answer this question.

The objective of this paper is to map, compare and improve the metastability margins for two converter topologies.

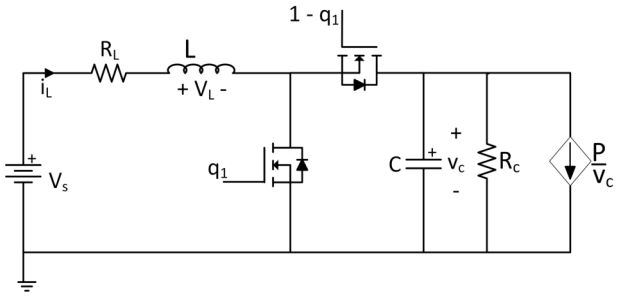

Fig. 1. Boost converter with a linear inductor with a pulsed power load

This paper will first present the converter topology used in previous research to map the metastability margins for pulse power loads. Then dual winding magnetic topology will be applied. Simulations will be presented to compare the response between the new and old topologies. Finally, metastabilty margins will be mapped and compared over a range of parameters of the pulse power load for new and old topologies.

II. Converter Model

A linear inductor boost converter topology seen in Figure 1 is used to map the metastability margins in previous research. The average mode model is used to express the duty cycle control for the simulations. The model for this converter is

$$L\,\frac{di_L}{dt} = V_s - i_L R_L - (1-d_1)v_c \tag{1}$$

$$C\,\frac{dv_c}{dt} = (1-d_1)i_L - \frac{v_c}{R_c} - \frac{P(t)}{v_c} \tag{2}$$

where, L is the inductance, R_L is the inductor's parasitic resistance, i_L is the inductor current, v_c is the output voltage, V_s is the input voltage, R_c is the stabilizing resistor, d_1 is the duty cycle of the switch 'q1', and $P(t)$ denotes the pulsed power. In Figure 2, P is the power level, Tp is the time period of the pulse and Dp is the duty cycle of the pulse.

III. Proposed Solution

Pulse power loads are a series of step changes in load. If the converter's dynamic characteristics can be improved for step changes in load, an attempt can be made to improve

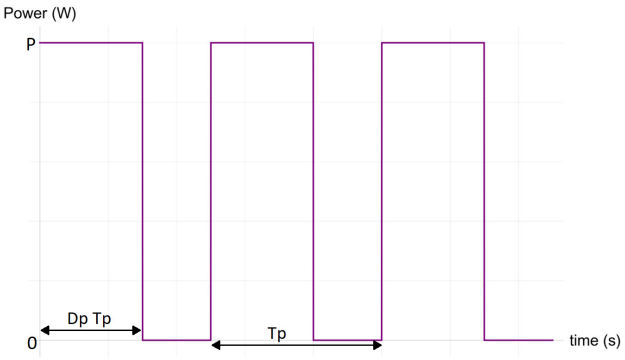

Fig. 2. Pulsed power loads

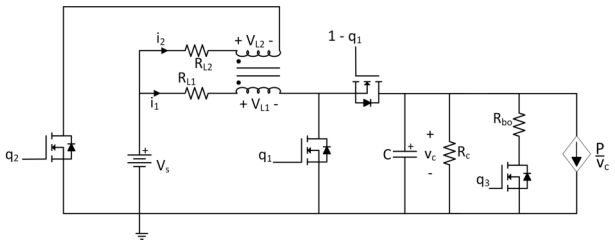

Fig. 3. Boost converter with a coupled inductor and a bleed off resistor with a pulsed power load

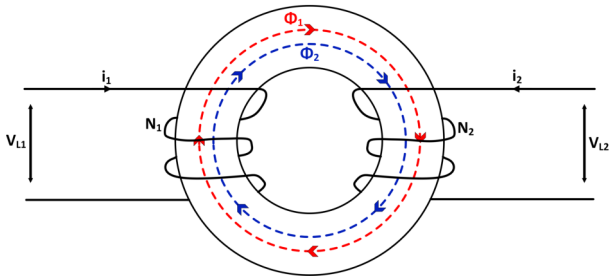

Fig. 4. Coupled inductor

the metastability margins with the new topology and control technique.

Dynamic characteristics for step changes in load can be improved with the Coupled Inductor Bleed-off Resistor topology i.e. the CIBR topology [7], [8].

Transition times between steady states are minimized with bang-bang control and can be further improved with a nonlinear saturating inductor model [9], [10]. Transition times are improved with a coupled inductor for step increase in loads and are improved with a bleed-off resistor for step decrease in loads [8]. The CIBR topology can be seen in Figure 3. The model for the coupled inductor can be seen in Figure 4.

Assuming that all flux created by each of the coils contributes towards saturating the inductor core, no leakage and nonlinear anhysteretic behavior [10], [11], the coupled inductor core in Figure 4 is analyzed. The equations that describe the core can be given as [8]

$$\frac{\lambda_{11}}{N_1} + \frac{\lambda_{22}}{N_2} = A_c\, a\, \arctan\left(b\left(\frac{N_1\, i_1}{l_c} + \frac{N_2\, i_2}{l_c}\right)\right) \tag{3}$$

$$\frac{\lambda_{11}}{N_1} - \frac{\lambda_{22}}{N_2} = A_c\, a\, \arctan\left(b\left(\frac{N_1\, i_1}{l_c} - \frac{N_2\, i_2}{l_c}\right)\right) \tag{4}$$

$$\frac{d\lambda_{11}}{dt} = \frac{N_2\, V_{L_1} - k\, N_1\, V_{L_2}}{(1-k^2)N_2} \tag{5}$$

$$\frac{d\lambda_{22}}{dt} = \frac{N_1\, V_{L_2} - k\, N_2\, V_{L_1}}{(1-k^2)N_1} \tag{6}$$

where, λ_{11} and λ_{22} are the self flux linkages, coefficient of coupling is denoted by k, λ_1 and λ_2 are the flux linkages, a and b are material dependent constants, A_c is the cross sectional area of the inductor core, l_c is the effective magnetic path length of the inductor core, and N_1 and N_2 are the turns in the inductor coils.

Analyzing the converter shown in Figure 3 and applying Equations (3) through (6) results in the model for the new topology, which is given as [8]

$$V_{L_1} = V_s - i_1 R_{L_1} - (1-d_1)v_c \tag{7}$$

$$i_2 = q_2\left(\frac{V_s - V_{L_2}}{R_{L_2}}\right) \tag{8}$$

$$C\,\frac{dv_c}{dt} = (1-d_1)i_1 - q_3\left(\frac{v_c}{R_{bo}}\right) - \frac{v_c}{R_c} - \frac{P(t)}{v_c} \tag{9}$$

$$\frac{\lambda_{11}}{N_1} + \frac{\lambda_{22}}{N_2} = A_c\, a\, \arctan\left(b\left(\frac{N_1\, i_1}{l_c} + \frac{N_2\, i_2}{l_c}\right)\right) \tag{10}$$

$$\frac{\lambda_{11}}{N_1} - \frac{\lambda_{22}}{N_2} = A_c\, a\, \arctan\left(b\left(\frac{N_1\, i_1}{l_c} - \frac{N_2\, i_2}{l_c}\right)\right) \tag{11}$$

$$\frac{d\lambda_{11}}{dt} = \frac{N_2\, V_{L_1} - k\, N_1\, V_{L_2}}{(1-k^2)N_2} \tag{12}$$

$$\frac{d\lambda_{22}}{dt} = \frac{N_1\, V_{L_2} - k\, N_2\, V_{L_1}}{(1-k^2)N_1}. \tag{13}$$

where, R_c is the stabilizing resistor, d_1 is the duty cycle of the 'q1' switch, and $P(t)$ denotes the pulsed power. This mathematical model is used when 'q2' is ON. When 'q2' is OFF, the coupled inductor behaves like a typical nonlinear saturating inductor. This model is expressed as [8]

$$\frac{d\lambda_1}{dt} = V_s - i_1 R_{L_1} - (1-d_1)v_c \tag{14}$$

$$C\,\frac{dv_c}{dt} = (1-d_1)i_1 - q_3\left(\frac{v_c}{R_{bo}}\right) - \frac{v_c}{R_c} - \frac{P(t)}{v_c} \tag{15}$$

$$\frac{\lambda_1}{N_1} = A_c\, a\, \arctan\left(b\,\frac{N_1\, i_1}{l_c}\right). \tag{16}$$

Flux in an inductor core cannot change instantaneously, when 'q2' switches from ON to OFF, all flux in the core can only interact with the first coil causing a jump in i_1. Assuming a lossless transfer of energy, i_1 after the jump is calculated as [8]

$$i_1 = \frac{l_c}{b\, N_1}\, \tan\left(\frac{1}{A_c\, a}\left(\frac{\lambda_{11}}{N_1} + \frac{\lambda_{22}}{N_2}\right)\right). \tag{17}$$

TABLE I
INDUCTOR CORE PARAMETERS FOR T650-52

Parameter	Value
A_c	$0.00184m^2$
l_c	$0.399m$
a	1.0237875
b	0.0002189

The number of turns in each coil are calculated from their nominal inductances and inductor core parameters as

$$N = \sqrt{\frac{L_{nominal}\, l_c}{a\, b\, A_c^2}}. \tag{18}$$

The inductor core is modeled after the T650-52 part from the Micrometals' catalogue [12]. These parameters are presented in Table I.

A. Transition process for a CIBR boost converter for a step increase in load

Based on the transition process as described in [8], the transition process is divided into three phases. The first phase begins before the load change. In this phase, 'q2' is ON and 'q1' operates at a high duty cycle (89%). The objective of this phase is to make the currents in both coils equal. To find the time interval for this phase, the system is simulated in forward time with appropriate switch states until either i_2 is equal to the initial value of i_1, or v_c breaches the threshold of a voltage drop 2% beyond the nominal ripple.

$$t_i = \begin{cases} t_{i1=i2} & \text{if } vc_f \geq vc_{threshold} \\ t_{vc} & \text{if } vc_f < vc_{threshold} \end{cases} \tag{19}$$

where, t_i is the initialization time, $t_{i1=i2}$ is the time at which both currents are equal, t_{vc} is the time at which v_c breaches $vc_{threshold}$, vc_f is the value of v_c at $t_{i1=i2}$, and $vc_{threshold}$ is the value of the threshold voltage. In the second phase, both coils are ON, and in phase three, both coils are OFF. The time intervals for these phases are found by minimizing a cost function given as [8]

$$\begin{aligned} \min J(t_f, t_r) =& (v_c(t_f) - v_c(t_r))^2 \\ &+ w\left(\frac{\lambda_{11}(t_f)}{N_1} + \frac{\lambda_{22}(t_f)}{N_2} - \frac{\lambda_1(t_r)}{N_1}\right)^2 \end{aligned} \tag{20}$$

where, J is the cost function, t_f and t_r are the forward and reverse times respectively, $v_c(t_f)$, $\lambda_{11}(t_f)$, $\lambda_{22}(t_f)$ represent the forward trajectories, $v_c(t_r)$, $\lambda_1(t_r)$ represent the reverse trajectories, and w is the weight for flux trajectories. To focus on just the transition process, the power load and stabilizing resistor are replaced by just one load resistor, and the step change in load is expressed as

$$R_{load} = \begin{cases} R_{load,1} & t < t_t \\ R_{load,2} & \text{otherwise} \end{cases} \tag{21}$$

where, t_t is the time at which the transition takes place. The parameters used for simulating the transition process are shown in Table II. The plots for the simulation results can be seen in Figure 5 which shows i_1 and Figure 6 which shows v_c. Important performance metrics logged in the simulation are given in Table III.

TABLE II
PARAMETERS FOR SIMULATING A STEP INCREASE IN LOAD FOR A CIBR BOOST CONVERTER

Parameter	Value
V_s	200 V
R_{L_1}	1 $m\Omega$
R_{L_2}	1 $m\Omega$
$L_{1,nominal}$	1 mH
N_1	32
$L_{2,nominal}$	1 mH
N_2	32
C	1 mF
R_{bo}	8 Ω
$R_{load,1}$	32 Ω
$R_{load,2}$	8 Ω
t_t	0.001 s
$f_{sw,q1}$	10 kHz
$v_{c,ref}$	400 V

TABLE III
PERFORMANCE METRICS FROM THE SIMULATION OF A STEP INCREASE IN LOAD FOR A CIBR BOOST CONVERTER

Performance metric	Value
Transition time	247.9 μs
Peak i_1	237.9 A
Minimum v_c	391 V

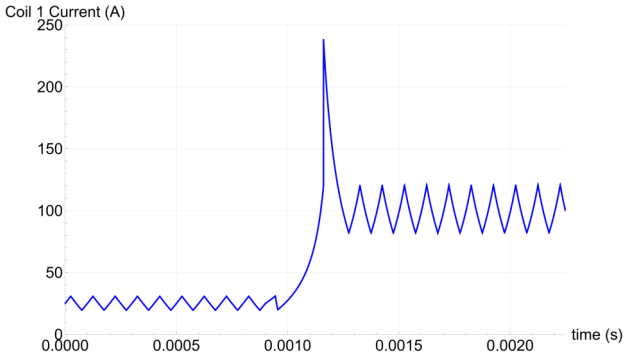

Fig. 5. i_1 in CIBR boost converter for a step increase in load

B. Transition process for a CIBR boost converter for a step decrease in load

Based on the transition process as described in [8], the transition process is divided into two phases. For the first phase of the transition process, 'q3' is ON and 'q1' is OFF. In the second phase of the transition process, both 'q1' and 'q3' are OFF. After the transition, the converter reverts to duty cycle control.

The time intervals for the two phases can be found by minimizing a cost function given as [8]

$$\min J(t_f, t_r) = (v_c(t_f) - v_c(t_r))^2 + (i_1(t_f) - i_1(t_r))^2 \tag{22}$$

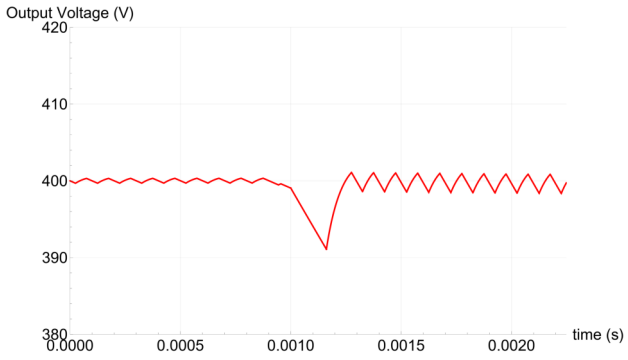

Fig. 6. v_c in CIBR boost converter for a step increase in load

TABLE IV
PARAMETERS FOR SIMULATING A STEP DECREASE IN LOAD FOR A CIBR BOOST CONVERTER

Parameter	Value
V_s	200 V
R_{L_1}	1 $m\Omega$
R_{L_2}	1 $m\Omega$
$L_{1,nominal}$	1 mH
N_1	32
$L_{2,nominal}$	1 mH
N_2	32
R_{bo}	8 Ω
C	1 mF
$R_{load,1}$	8 Ω
$R_{load,2}$	32 Ω
t_t	0.0005 s
$f_{sw,q1}$	10 kHz
$v_{c,ref}$	400 V

TABLE V
PERFORMANCE METRICS FROM THE SIMULATION OF A STEP DECREASE IN LOAD FOR A CIBR BOOST CONVERTER

Performance metric	Value
Transition time	191.7 μs
Minimum i_1	N/A
Peak v_c	N/A

where, $v_c(t_f)$ and $i_1(t_f)$ represent the forward time trajectories, and $v_c(t_r)$ and $i_1(t_r)$ represent the reverse time trajectories. An important factor to be noted is that the bleed off resistor needs to have such a value that when aggregated with the new load, they need to be larger than the load the converter is transitioning from. The parameters used for simulating the transition process are shown in Table IV. The plots for the results of the simulation of the transition process can be seen in Figure 7 which shows i_1 and Figure 8 which shows v_c. Important performance metrics logged in the simulation are given in Table V. As the current follows a direct trajectory between steady states and the voltage deviation is within the steady state ripple, the performance metrics of minimum i_1 and peak v_c are not applicable in Table V.

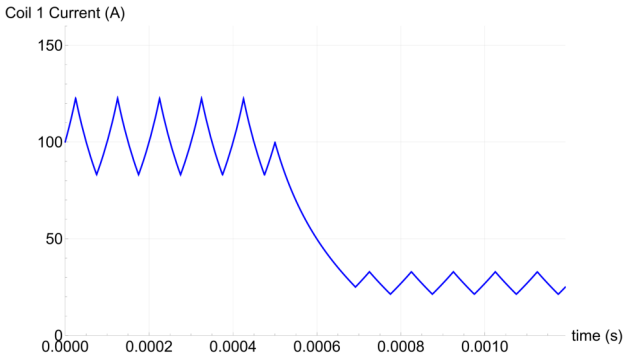

Fig. 7. i_1 in CIBR boost converter for a step decrease in load

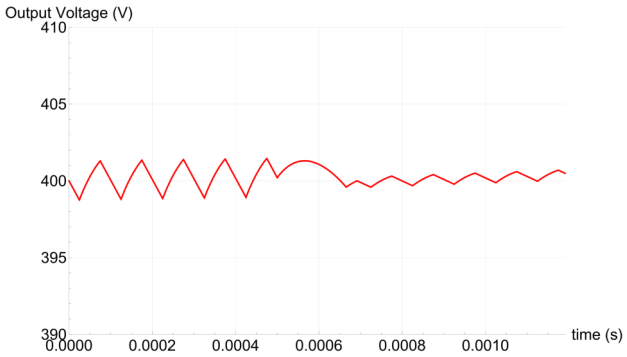

Fig. 8. v_c in CIBR boost converter for a step decrease in load

IV. SYSTEM BEHAVIOR AND METASTABILITY MAPS

This section shows the stability maps for a boost converter with a linear inductor model and a CIBR boost converter when connected to a pulsed power load. The first subsection demonstrates through simulations the behavior of a boost converter with a linear inductor model with duty cycle control when the system is stable and when it is unstable. The second subsection demonstrates through simulations the behavior of a CIBR boost converter with bang-bang control when the system is stable and when it is unstable. The third and final subsection compares the stability maps obtained using both topologies.

A. Stability map for a boost converter with a linear inductor

The parameter values used for conducting the simulations to demonstrate the system's behavior and to map the stability margins are listed in Table VI. In this paper, stability is determined from the behavior of the system's states. The boost converter with a linear inductor model behaves in specific ways with constant duty cycle control when the system is stable and unstable. When the system is stable, the inductor current and output voltage have consistent bounded oscillations. This behavior can be seen in Figure 9 and Figure 10. When the system is unstable, the oscillations in the inductor current keep growing without bounds with each power pulse and the output voltage collapses to zero after a rapid growth in the amplitude of its oscillations. This behavior can be seen in Figure 11

TABLE VI
PARAMETERS FOR SIMULATING A BOOST CONVERTER WITH A LINEAR INDUCTOR WITH A PULSED POWER LOAD

Parameter	Value
V_s	200 V
R_L	1 $m\Omega$
L	1 mH
C	1 mF
R_c	50 Ω
$v_{c,ref}$	400 V Ω
d_1	0.5

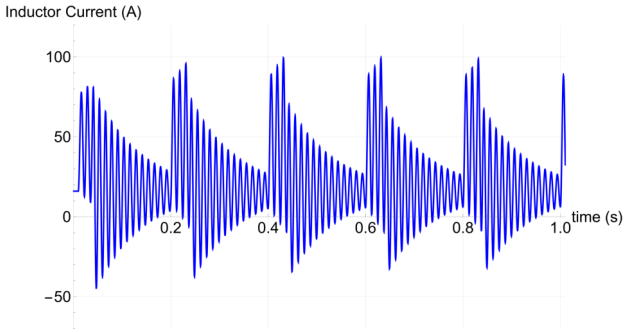

Fig. 9. Inductor current for boost converter with a linear inductor with a pulsed power load when system is stable ($P = 6kW, Tp = 0.2s, Dp = 0.2$)

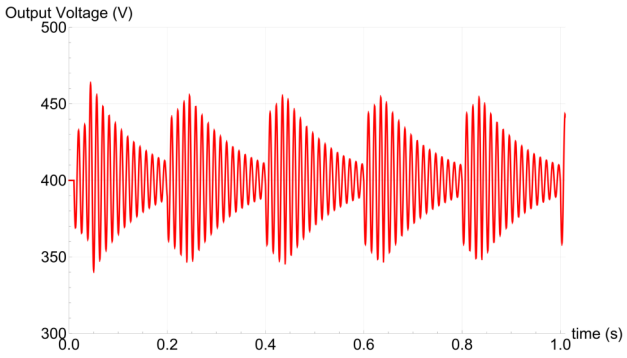

Fig. 10. Output voltage for boost converter with a linear inductor with a pulsed power load when system is stable ($P = 6kW, Tp = 0.2s, Dp = 0.2$)

and Figure 12. These simulations demonstrating stable and unstable behavior have the pulse power level set at 6kW and the pulse power time period set at 0.2s. The pulse power duty cycle of 0.2 is stable and the pulse power duty cycle of 0.6 is unstable. From this behavior, it can be concluded that whether the system is unstable can be determined by surveilling the output voltage. Thus, the system can be classified as unstable by detecting a steady increase in the maximum amplitude of its oscillation for five power pulses or by detecting the output voltage collapsing to zero, whichever comes first. If this criterion is not satisfied, the system is classified as stable.

The stability margins are mapped by detecting the maximum duty cycle of the pulsed power for which the system is stable over a range of power levels and time periods for the pulsed power load. The stability map for the boost converter with

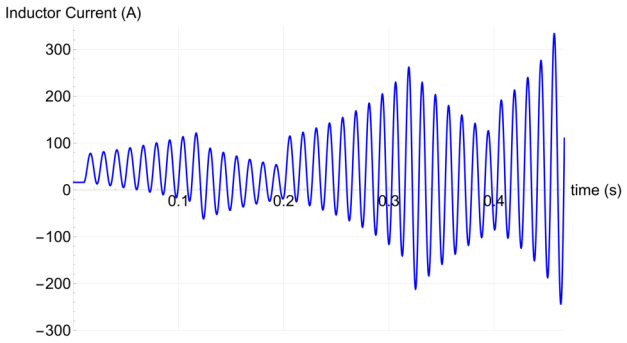

Fig. 11. Inductor current for boost converter with a linear inductor with a pulsed power load when system is unstable ($P = 6kW, Tp = 0.2s, Dp = 0.6$)

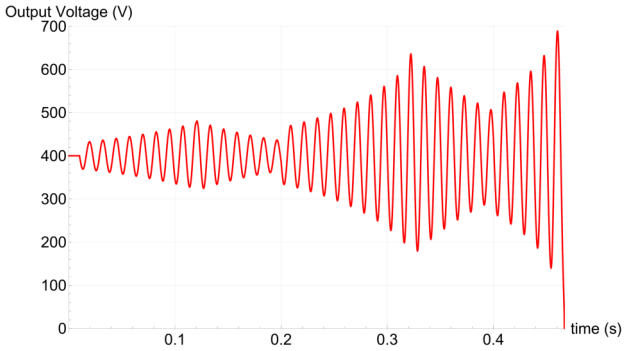

Fig. 12. Output voltage for boost converter with a linear inductor with a pulsed power load when system is unstable ($P = 6kW, Tp = 0.2s, Dp = 0.6$)

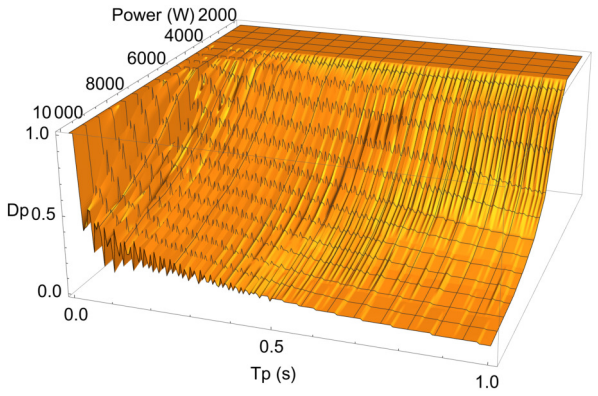

Fig. 13. Stability map for boost converter with a linear inductor with a pulsed power load

a linear inductor model and constant duty cycle control can be seen in Figure 13. The stability margins trend down as power level increases for a certain time period. Also, there are fluctuations in the margins with respect to the time period for a constant power level.

B. Stability map for a CIBR boost converter

The parameter values used for conducting the simulations to demonstrate the system's behavior and to map the stability

TABLE VII
PARAMETERS FOR SIMULATING A CIBR BOOST CONVERTER WITH A PULSED POWER LOAD

Parameter	Value
V_s	200 V
R_{L_1}	1 $m\Omega$
R_{L_2}	1 $m\Omega$
$L_{1,nominal}$	1 mH
N_1	32
$L_{2,nominal}$	1 mH
N_2	32
C	1 mF
R_{bo}	16 Ω
R_c	50 Ω
$v_{c,ref}$	400 V Ω

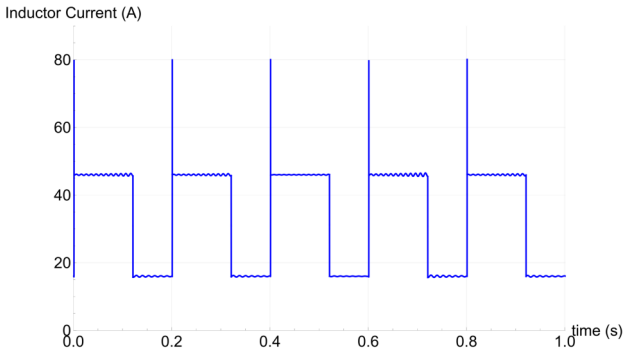

Fig. 14. Inductor current for CIBR boost converter with a pulsed power load when system is stable ($P = 6kW, Tp = 0.2s, Dp = 0.6$)

margins are listed in Table VII. The CIBR boost converter in conjunction with bang-bang control behaves in certain ways when the system is stable and unstable. When the system is stable, the inductor current and output voltage have bounded oscillations and may have fluctuations in the maximum amplitude for each power pulse for some sets of parameters. This behavior can be seen in Figure 14 and Figure 15. When the system is unstable, the oscillations in the inductor current keep growing without bounds with each power pulse and so do the oscillations in the output voltage. This behavior can be seen in Figure 16 and Figure 17. These simulations demonstrating stable and unstable behavior have the pulse power level set at 6kW and the pulse power time period set at 0.2s. For a CIBR converter, the pulse power duty cycle of 0.6 is stable and the pulse power duty cycle of 0.8 is unstable. From this behavior, it can be concluded that whether the system is unstable can be determined by surveilling the output voltage. Thus, the system can be classified as unstable by detecting a steady increase in the maximum amplitude of its oscillation for five power pulses. If this criterion is not satisfied, the system is classified as stable.

Similar to the process of mapping the stability margins seen previously, the margins are mapped by detecting the maximum duty cycle of the pulsed power for which the system is stable over a range of power levels and time periods for the pulsed power load. The stability map for the CIBR boost converter

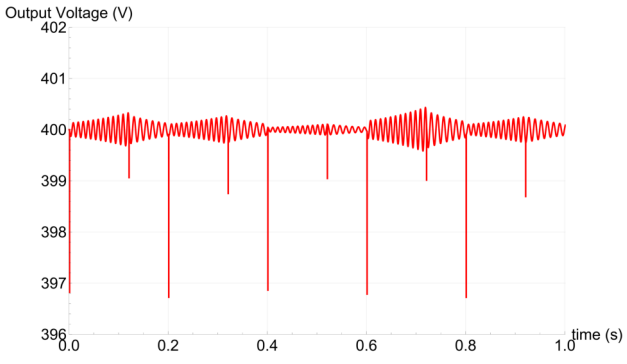

Fig. 15. Output voltage for CIBR boost converter with a pulsed power load when system is stable ($P = 6kW, Tp = 0.2s, Dp = 0.6$)

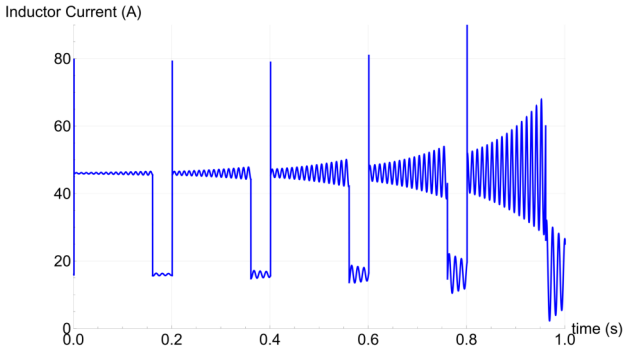

Fig. 16. Inductor current for CIBR boost converter with a pulsed power load when system is unstable ($P = 6kW, Tp = 0.2s, Dp = 0.8$)

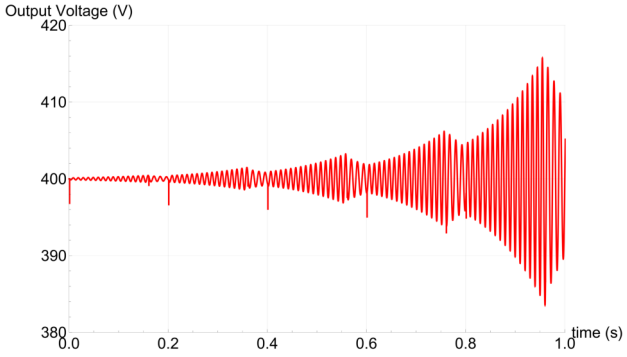

Fig. 17. Output voltage for CIBR boost converter with a pulsed power load when system is unstable ($P = 6kW, Tp = 0.2s, Dp = 0.8$)

and bang-bang control can be seen in Figure 18. Even though the results are quantitatively different when compared to the previous map, qualitatively they are very similar. The stability margins trend down as power level increases for a certain time period, and there are fluctuations in the margins with respect to the time period for a constant power level.

C. Comparison of the stability maps

The plot for the comparison of the stability maps for the linear inductor boost converter and the CIBR boost converter

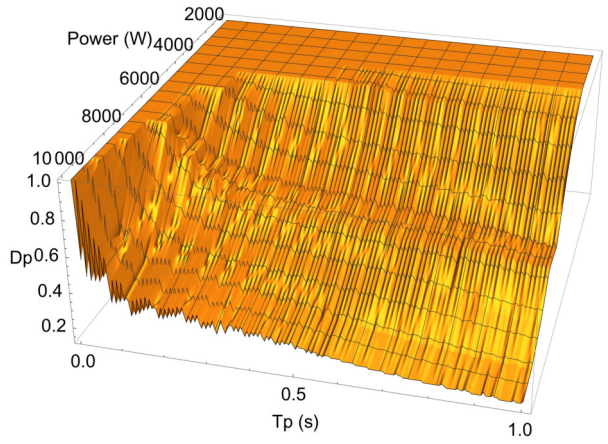

Fig. 18. Stability map for CIBR boost converter with a pulsed power load

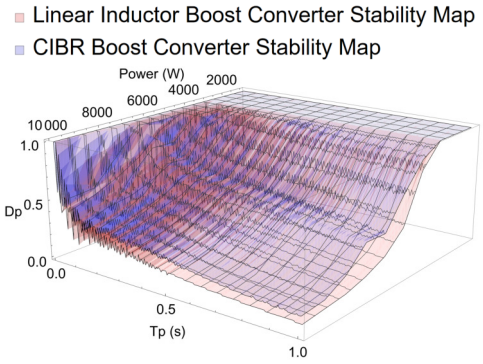

Fig. 19. Comparison of the stability maps

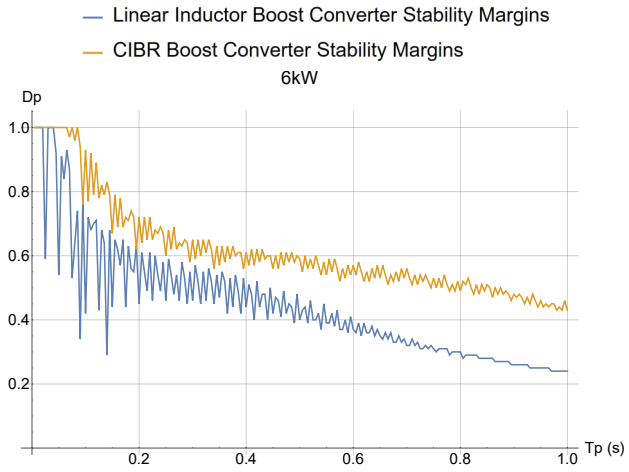

Fig. 20. A slice of Figure 19 at 6kW

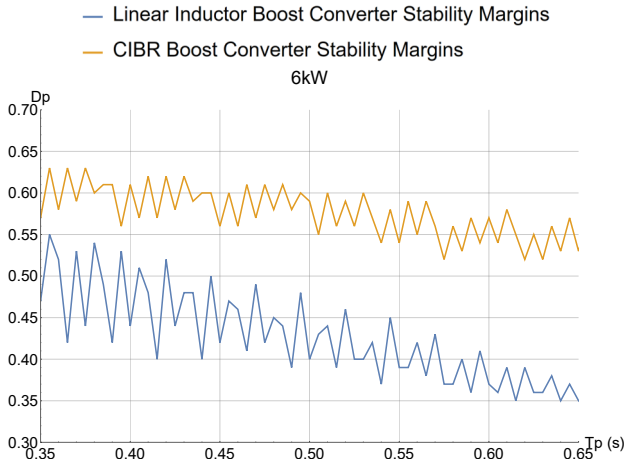

Fig. 21. Zoomed in version of Figure 20

can be seen in Figure 19. A slice of this comparison plot at 6kW can be seen in Figure 20. A plot that shows the ripples in the stability margins in more detail can be seen in Figure 21. Figures 20 and 21 show that the boundary of the stability margin has ripples that could determine the operational regions for a system. If a certain load has a constant power level and constant pulse duty cycle with varying time periods, the system may not be stable at all operating points. The system parameters determine when and how the system reacts to the load and changes in the load, and the load parameters determine when and how the load switches. Thus, if any system parameter is changed, a change is expected in the stability margin and the ripple seen in the stability margin. The stability margins and the ripples in the boundaries of the stability margins are different for three different nominal inductance values for a CIBR boost converter connected to a pulsed power load whose power level is at 5kW. Figure 22 shows that the stability margins and the ripples seen in the stability margins change when any system parameter is changed. As the nominal inductance increases, the width of the ripple increases and the average stability decreases. Thus, it can be confidently said that the ripple in the stability margin boundary must be a result of the system parameters and the parameters of the pulsed power, although a quantifiable relationship is hard to derive due to the numerical nature of the simulations.

Two thousand data points can be extracted if the stability margins are inspected at $1kW$ intervals for P and $0.005s$ intervals for Tp. For this sample size of two thousand data points, the average increase in the stability margins due to the CIBR topology and bang-bang control is 38%. This is a substantial average improvement in the stability margins.

V. Conclusion

This paper presents a different topology and control strategy to improve the metastability margins for pulse power loads. The average increase in the metastability margin is substantial. The disadvantage is the added hardware required for the new topology. In conclusion, numerical simulations show that the CIBR topology in conjunction with bang-bang control improves the metastability margins for pulse power loads by 38%.

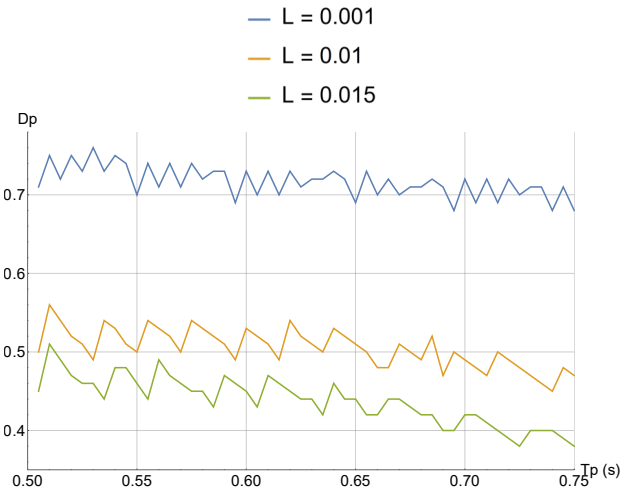

Fig. 22. Stability margins for different nominal inductances for a CIBR boost converter with a pulsed power load ($P = 5kW$)

VI. Acknowledgment

Sandia National Laboratories is a multi-mission laboratory managed and operated by National Technology and Engineering Solutions of Sandia, LLC., a wholly owned subsidiary of Honeywell International, Inc., for the U.S. Department of Energy's National Nuclear Security Administration under contract DE-NA0003525. This paper describes objective technical results and analysis. Any subjective views or opinions that might be expressed in the paper do not necessarily represent the views of the U.S. Department of Energy or the United States Government.

References

[1] V. Salehi, B. Mirafzal, and O. Mohammed, "Pulse-load effects on ship power system stability," in *IECON 2010 - 36th Annual Conference on IEEE Industrial Electronics Society*, 2010, pp. 3353–3358.

[2] R. Bartelt, M. Oettmeier, C. Heising, V. Staudt, and A. Steimel, "Scenario-based stability-assessment of converter-fed dc-ship grids loaded with pulsed power," in *2011 IEEE Electric Ship Technologies Symposium*, 2011, pp. 468–471.

[3] H. Smolleck, S. Ranade, N. Prasad, and R. Velasco, "Effects of pulsed-power loads upon an electric power grid," *IEEE Transactions on Power Delivery*, vol. 6, no. 4, pp. 1629–1640, 1991.

[4] R. D. R. III and D. G. Wilson, *Nonlinear Power Flow Control Design*. Springer London, 2011. [Online]. Available: https://doi.org/10.1007/978-0-85729-823-2

[5] W. W. Weaver, R. D. Robinett, D. G. Wilson, and R. C. Matthews, "Metastability of pulse power loads using the hamiltonian surface shaping method," *IEEE Transactions on Energy Conversion*, vol. 32, no. 2, pp. 820–828, 2017.

[6] J. A. Dillon, W. W. Weaver, R. D. Robinett, and D. G. Wilson, "Electro-mechanical-thermal performance and stability of aircraft energy networks with pulse power loads," *IEEE Transactions on Aerospace and Electronic Systems*, vol. 56, no. 4, pp. 2537–2547, 2020.

[7] C. S. Inamdar, "Dynamic characteristics of dc-dc converters with coupled and nonlinear magnetics," M.S. thesis, Department of Electrical and Computer Engineering, Michigan Technological University, Houghton, MI, USA, 2021.

[8] C. S. Inamdar and W. W. Weaver, "Input shaping control of dc-dc converters with nonlinear coupled magnetics," in *2022 IEEE Power and Energy Conference at Illinois (PECI)*, 2022, pp. 1–8.

[9] S. V. Dhople, K. A. Kim, and A. D. Domínguez-García, "Time-optimal control in dc-dc converters: A maximum principle perspective," in *2014 IEEE Applied Power Electronics Conference and Exposition - APEC 2014*, 2014, pp. 2804–2808.

[10] J. T. Lukowski, W. W. Weaver, and R. D. Robinett, "Time-optimal input-shaping control of a saturating inductor dc-dc converter," in *2018 IEEE 19th Workshop on Control and Modeling for Power Electronics (COMPEL)*, 2018, pp. 1–5.

[11] M. Takach and P. Lauritzen, "Survey of magnetic core models," in *Proceedings of 1995 IEEE Applied Power Electronics Conference and Exposition - APEC'95*, vol. 2, 1995, pp. 560–566 vol.2.

[12] "Curve fit formulas and values - design tools - micrometals," https://www.micrometals.com/design-and-applications/design-tools/, accessed: 2020-06-14.